

Simulation of Site-Selective Etching by Invoking Effects of Ligands and Reactant Diffusion

Guangyu He, An Su, Qian Wang, Shi Liu, and Hongyu Chen*



Cite This: *J. Phys. Chem. Lett.* 2025, 16, 7069–7075



Read Online

ACCESS |



Metrics & More

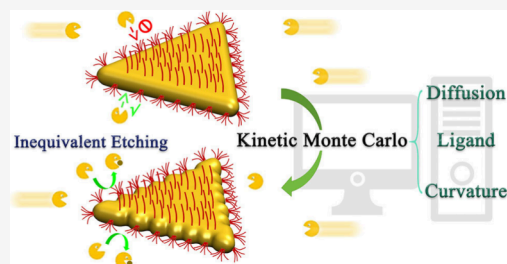


Article Recommendations



Supporting Information

ABSTRACT: We explore the origin of inequivalent etching on equivalent crystal sites by developing a kinetic Monte Carlo model. This new model focuses on the effects of both the diffusion of reactants and ligands, factors that are ubiquitous in wet-chemistry experiments and yet often overlooked or oversimplified in conventional simulations, where the defaults are rapid reactant redistribution and rapid equilibration of ligand adsorption/desorption. Our results show the dramatic differences arising from non-equilibrium ligand control, which cause selective etching at the corners, edges, or facets of Au triangular nanoplates. Basically, the ligand effects provide a positive feedback when etching targets the ligand-deficient sites, and the newly exposed atoms are ligand-free. In contrast, slow reactant diffusion provides a negative feedback, as a reactive site cannot etch unrestrictedly due to the lack of reactants. The dynamic competitions are clearly manifested in the focused etching mode when ligand effects coincide with large diffusion rates. By appropriately setting these two crucial factors, we reproduce *in silico* a series of etching products that are fully consistent with previous experimental results, along with the details in the shape of notches at the edges and holes on the plane. We believe that our simulation model could be expanded to many other systems and provide detailed inner workings for the mechanisms of abnormal crystal morphologies.



Synthetic development of nanocrystals is of fundamental importance for the advance of nanotechnology as it provides the initial innovation of materials for functional exploration. Other than experimental studies of synthetic methods, a vital alternative is computational simulation, which, with the suitable parameters, could unveil the kinetic details of various processes, such as morphological transformation and ligand-specific facet control.^{1–5}

Previous simulations often downplay the role of ligands in the morphological evolution of nanocrystals^{2,6,7} while assuming that the diffusion rate of reactants is sufficiently fast to reach near-equilibrium.^{2,4–7} Thus, the reactants could be described by constant chemical potentials. Under near-equilibrium conditions, this approach has been rather effective in predicting the most stable facets in a wide range of materials^{8–10} and even helical structures by introducing screw dislocation.^{11,12}

However, abnormal growth modes beyond facet control have been reported, for example, the dendritic growth of snowflakes,^{13–15} the growth of a long “tail” from the initially equivalent side facets of Ag nanoplates,¹⁶ or the formation of raised ridges and deep valleys from initially flat Au nanoplates.¹⁷ Notably, in these cases, the equivalent sites do not grow equivalently, which cannot be explained within the aforementioned framework. Thus, more factors should be taken into consideration to fully account for the growth modes in these systems,¹⁸ perhaps by invoking nonuniform reactant distribution and/or ligand effects.

Nonuniform diffusion has been studied in the dendritic growth of snowflakes.^{19–21} Evidently, this growth mode deviates from traditional theories of crystal growth, where branching is not favored. By incorporation of diffusion into a Monte Carlo model, Gravner et al. successfully simulate the formation of snowflakes with diverse morphologies.^{19,20} However, this approach has rarely been applied to crystal growth in solution.

The conventional treatment of ligands involves calculating their adsorption energies on different crystal facets, and the facet having the largest adsorption energy is considered as the dominant one in the ultimate morphology.^{4,5} We have concerns over these simplified treatments, as the packing of strong ligands takes time,²² and the resulting nonuniform distribution would certainly affect material deposition. Therefore, it is essential to incorporate dynamic ligand conditions into simulation of wet-chemistry material synthesis, particularly for strong ligands during rapid growth.

In our past study of active surface growth or etching, we have come to know the enormous impact of ligand effects.^{23–26}

Received: April 28, 2025

Revised: June 21, 2025

Accepted: June 30, 2025

Of close relevance to this work, by pre-coverage of strong ligands and removal of the excess ones, we could focus etching to occur at the supposed ligand-deficient side edges or the flat region of Au nanoplates, giving serrated edges²⁴ or holes,²⁵ respectively. Such an inequivalent etching of initially equivalent sites cannot be explained by conventional arguments.

Hence, we postulate that both ligand effects and diffusion should be taken into consideration. To computationally model such an active surface etching, here, we develop a new algorithm framework based on kinetic Monte Carlo (KMC). The effect of the adsorbed ligand is presented in numerical form and correlated to the probability of the reaction occurring at an individual lattice point. We endeavor to construct the model with minimal key parameters, such as the reaction activation barrier, amount of reactant, and diffusion, all of which hold significant physical and chemical implications. This dynamic simulation allows us to study crystal growth and etching under ligand control and, thus, to track unconventional morphological evolution, such as the site-selective etching at the corners, edges, and top facets of triangular Au nanoplates.

In contrast to describing the solution phase by a chemical potential, we utilize a discrete model, which is suitable to reproduce the local differences of the reactant distribution. In this model, each lattice point is set as either occupied with one atom (marked by 1, the Au point) or unoccupied (marked by 0, the environment point). In addition, the diffusion of reactants, including reactant precursor and etching agent, takes place merely between the adjacent environment points as opposed to real continuous media.

For reactions at each lattice point, two events ($0 \rightarrow 1$ and $1 \rightarrow 0$) are considered, representing the process of growth or etching. The occurrence of these events is evaluated using the reaction rate τ obtained through the Eyring equation^{27,28}

$$\tau = \nu e^{-\Delta G^\ddagger/kT} \quad (1)$$

where ν is the frequency factor (approximated as a constant under the same reaction conditions), k is the Boltzmann constant, T is the reaction temperature, and ΔG^\ddagger is the activation energy of the reaction. Because obtaining high-accuracy ΔG^\ddagger is complicated and unnecessary for the issues of our concern,²⁹ it is determined in a simple way. First, we approximate the reaction energy ΔE by counting bonding numbers and fitting precalculated empirical data (see the [Supporting Information](#) for more details).^{30–32} Subsequently, ΔG^\ddagger is calculated based on the Bell–Evans–Polanyi (BEP) relation,^{33–35} which suggests that reactions of a similar nature would follow the same linear relationship between ΔE and ΔG^\ddagger . Hence, ΔG^\ddagger of event $1 \rightarrow 0$ is expressed as

$$\Delta G^\ddagger = f_1 \Delta E \quad (2)$$

where f_1 is affected by the reaction condition, determining the relative probability of events under different environments of bonding.

ΔG^\ddagger of growth event $0 \rightarrow 1$ mainly refers to the reduction of the precursor and overcoming the constraints imposed by ligands. We set a correlation between the bonding number and ΔE for event $0 \rightarrow 1$ by mirroring the fitted values of event $1 \rightarrow 0$ (Figure S2). Similarly, its ΔG^\ddagger is assumed to satisfy

$$\Delta G^\ddagger = f_2 \Delta E \quad (3)$$

Apart from the factors that have been involved in eq 1, Sekerka suggests that the corner sites of the crystal have a larger

effective reactant concentration in comparison to the planar sites,³⁶ for a higher chance of colliding with the reactant on a spatial scale. This argument is commonly invoked to explain the formation of concave structures from initially flat planes.^{37,38} Notably, the current discrete model is suitable to describe the effect of different collision probability by summing up all of the amount of reactant a_i of each reaction site's adjacent environment point i as a_{tot} . Then, the Eyring equation is expressed as

$$\tau = a_{\text{tot}} \nu e^{-\Delta G^\ddagger/kT} \quad (4)$$

Specially, the detailed components of a_{tot} for two events are slightly different, eq 5 for event $0 \rightarrow 1$ and eq 6 for event $1 \rightarrow 0$, where a_{reac} is the amount of reactant for the reaction site and $N_{\text{env_adj}}$ corresponds to the set of environment points adjacent to the reaction site.

$$a_{\text{tot}} = a_{\text{reac}} + \sum_{i \in N_{\text{env_adj}}} a_i \quad (5)$$

$$a_{\text{tot}} = \sum_{i \in N_{\text{env_adj}}} a_i \quad (6)$$

As the reactions consume the reactant, leading to uneven distribution, it would be constantly replenished under the driving force of a concentration gradient. To appropriately describe these processes, we carried out the simulation with the amount of reactant dynamically adjusted (the ARDA condition).

At first, each environment point i would be allocated an initial amount of reactant designated as $a_{i,0}$. As the simulation proceeds from state $s - 1$ to s , the occurrence of the event would consume the reactant of each adjacent environment point i ($a_{i,s-1}$), and a redistributed amount of reactant $a_{i,s}^{\text{red}}$ is given by

$$a_{i,s}^{\text{red}} = (a_{\text{tot},s-1} - 1) / n_{\text{env_adj},s} \quad (7)$$

which would be assigned to the involved environment points. Other points are dealt with by $a_{i,s}^{\text{red}} = a_{i,s-1} \cdot a_{\text{tot},s-1}$ for event $0 \rightarrow 1$ is expressed as eq 8, while event $1 \rightarrow 0$ is written as eq 9. Among them, $n_{\text{env_adj},s}$ is the number of adjacent environment points to the reaction site of state s .

$$a_{\text{tot},s-1} = a_{\text{reac},s-1} + \sum_{i \in N_{\text{env_adj},s-1}} a_{i,s-1} \quad (8)$$

$$a_{\text{tot},s-1} = \sum_{i \in N_{\text{env_adj},s-1}} a_{i,s-1} \quad (9)$$

As such, the uneven distribution of reactants leads to the diffusion between adjacent environment points. The amount of the reactant after diffusion for each environment point i ($a_{i,s}$) is calculated according to its amount of reactant $a_{i,s}^{\text{red}}$, and the amount of reactant for lattice point j ($a_{j,s}^{\text{red}}$) belongs to adjacent lattice points ($N_{\text{adj},s}$) and factor D (ranging from 0 to 1 as a measure of the diffusion rate),²⁰ expressed as

$$a_{i,s} = (1 - D) a_{i,s}^{\text{red}} + D \sum_{j \in N_{\text{adj},s}} a_{j,s}^{\text{red}} / 12 \quad (10)$$

Specially, $a_{j,s}^{\text{red}} = a_{i,s}^{\text{red}}$ when the adjacent lattice point j is the Au point.

The inherent complexity of ligands poses significant challenges for existing simulation methods to fully account

for their roles during crystal growth or etching. To address this, it is necessary to introduce certain simplifications of ligand behavior to make the simulations computationally feasible. We believe that the strength of interaction between the ligand and surface atom, ligand packing, or hydrogen-bonding interactions between ligands, for the purpose of controlling growth and etching, essentially reduces the reactivity of the corresponding surface atoms. Describing the influence of ligands through their impact on activation energy has also been employed in other studies to elucidate the mechanisms underlying the selective growth of crystals at corners, edges, and facets.³⁹ Thus, we assign a numerical value, denoted as l_i , to each surface Au point i . The value of l_i increases with the strength of the interaction between the ligand and the surface atom. For cases where the ligand can fully adsorb onto the crystal surface, a larger l_i value is assigned, indicating that the corresponding atom is effectively protected by the ligand and is typically resistant to etching. However, as neighboring atoms are progressively etched away, the protective effect of the ligand gradually weakens. Additionally, under the assumption that the fewer the bonding number of an atom (n_{bond}), the stronger ligand binds to the atom, l_i is set as $1.0 + 0.1 \times (12 - n_{\text{bond}})$. To mimic the passivating effects, the rate equation is written as

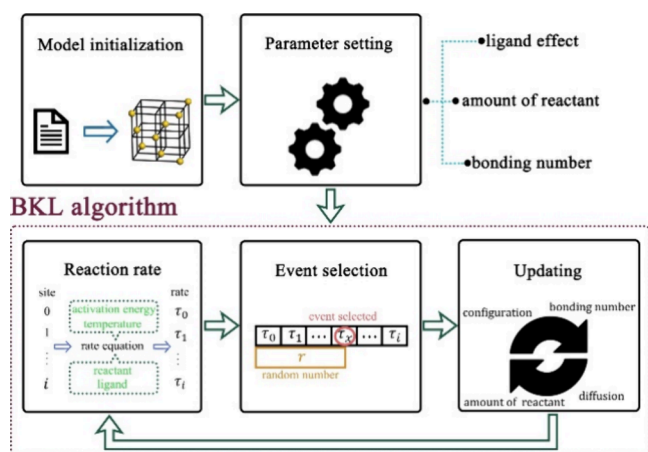
$$\tau = a_{\text{tot}} \nu e^{-\Delta G^\ddagger(1+\ln l)/kT} \quad (11)$$

To prevent overlap during the etching process, where two expanding etching sites could merge into a single larger site (see the Supporting Information for more details), the preferential etching sites generated by the uneven distribution of ligands are selected manually, and each site involves several adjacent surface Au points, which are assigned with small l_i ($l_i = 1.00$ or 1.10), representing weak ligand passivation, due to either ligand loss or a defect in the ligand layer. It is worth mentioning that, in the experimental setup, the concentration of residual ligand in the solution is very low, as the nanoplates were repeatedly purified to remove the excess ligands.^{24,25} Therefore, there would be few ligands binding to the newly exposed atoms during etching, and their ligand effects are ignored in our simulation.

The overall procedure can be summarized as the following steps (Scheme 1, and see the Supporting Information for more details):

Step 1: Initializing the parameters of the Au and environment points.

Scheme 1. Overall Procedure of the Simulation



Step 2: Calculating the reaction rate τ_i for each site i within the set of reaction sites (N_{react}) and obtaining the rate sum τ_{tot} .

$$\tau_{\text{tot}} = \sum_{i \in N_{\text{react}}} \tau_i \quad (12)$$

Step 3: Determining which event takes place with a random number r (ranging from 0 to τ_{tot}) and τ_{tot} according to the Bortz–Kalos–Lebowitz algorithm.^{40,41}

Step 4: Proceeding with the event chosen leading to a new configuration.

Step 5: Updating the parameters of the new configuration.

Step 6: Repeating steps 2–5.

In this study, we constructed a triangular Au nanoplate of *fcc* lattice (Figure S1) with a “–ABC–ABC–A–CBA–CBA–” stacking sequence,^{42–44} bound by a twin plane in the middle (Figure 1 and Figure S3).^{44,45} The surface atoms could be

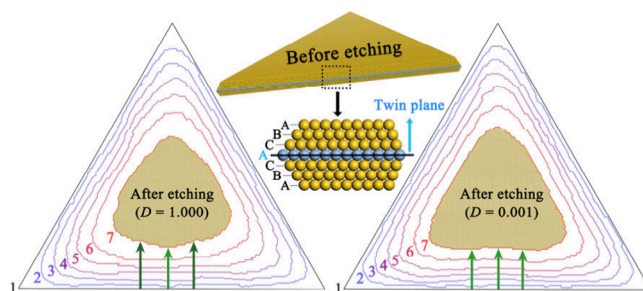


Figure 1. Etching of a triangular Au nanoplate in the absence of ligands under the ARDA condition, showing two cases with $D = 1.000$ (left panel) and 0.001 (right panel), respectively.

categorized as facet, edge, and corner sites according to their spatial position. Without considering the ligand effects, the stability of surface atoms decreases from facet to edge and then corner sites, as well agreed upon in the community. Using the triangular Au nanoplates, several distinct etching scenarios observed experimentally are investigated to validate our model.

First, we studied the etching of a triangular nanoplate excluding ligand effects (Figure 1). When the changing morphology was tracked, etching first took place at the corner sites and gradually extended to the edge sites. Thus, the etching at the corner sites was clearly more extensive than that at the edge sites, as shown by the gradually evolving boundary. With this difference accumulated, the triangular nanoplate gradually became rounder. As we reduced D (from 1.000 to 0.001), the product became less round, retaining a roughly triangle morphology. With the diminished D , meaning that the consumed reactants cannot be replenished in time, the process gradually turned into a layer-by-layer etching mode.

These results are similar to the experimental etching products in the absence of strong –SH-based ligands.^{24,25} That is, the weak ligands and surfactants undergo rapid adsorption/desorption dynamics, and thus, the etching would preferentially target the high-curvature corners, leading to corner-selective etching.

This system is far from equilibrium, and therefore, the roundness of the product nanoplate does not arise from the thermodynamic argument of globally minimal surface energy but from the kinetic aspect of higher reactivity for the corner sites.⁴⁶ It is worth mentioning that the current etching is not focused on a few active sites, as opposed to the following examples.

As discussed above, our previous work on the new etching modes depends critically on the initial coverage of strong ligands.²⁴ The triangular nanoplates are first incubated with 2-naphthalenthioi, and the excess ligands are then removed. As such, the high-curvature corners are better preserved by the ligands due to less steric packing and higher affinity. The relatively ligand-deficient sites, presumably due to site selectivity and random ligand desorption, are preferentially etched, giving serrated edges. The unusual etching mode is strong proof for the dominant role of ligands, in order to differentiate the active sites from the passivated ones. This scenario is in clear contrast to the above case, where the bonding number is the primary factor.

To generate a similar etching condition *in silico*, we assigned l_i to all surface Au points. In addition, we manually picked one active site at each edge of the triangular nanoplate (panels a–c of Figure 2) to represent the preferential etching sites. As

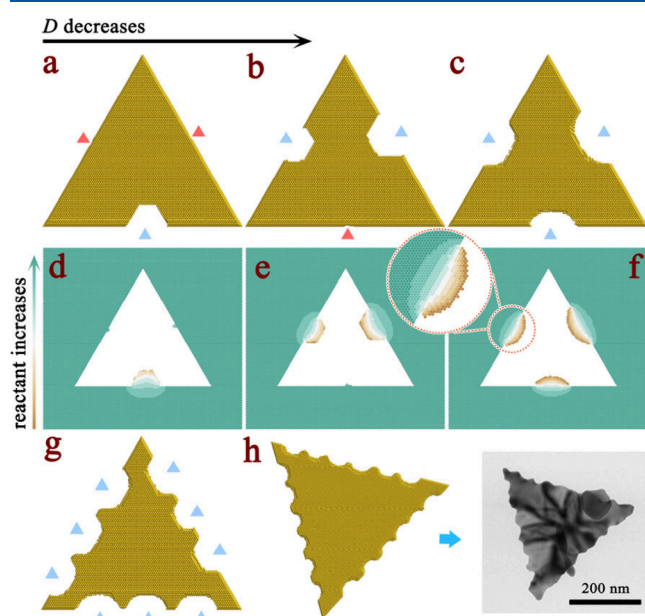


Figure 2. (a–c) Selective etching at the edge sites of a triangular Au nanoplate under the ARDA condition, with D decreasing for the representative three cases ($D = 0.150, 0.060, \text{ and } 0.030$). Initially, all surface atoms have ligands, and one site per each edge is assigned to be preferentially etched. Some of them are etched significantly (blue triangles), while others are barely etched (red triangles). (d–f) Reactant distribution at the same plane of the twin plane. The amount of reactant is shown by a gradient of colors ranging from cyan to brown, with the cyan color being the initial setting of the reactant. (g and h) Conditions are the same as panel c, except three or six sites per edge are assigned as the preferential sites. A transmission electron microscopy image is provided for comparison.

shown in panels a–c of Figure 2, the etching products were drastically different from the above case without a ligand. With D gradually decreased, an increasing number of notches were generated in the resulting products. More specifically, with the largest D among the three cases, only one site was etched, whereas with the smallest D , all three sites were equally etched. That is, with the same ligand effect and with etching starting simultaneously, a large D could focus etching at the relatively more active sites. Moreover, the notch in Figure 2a had facet-like edges; the notches in Figure 2c were an arc-shaped smooth

surface; and remarkably, the intermediate case in Figure 2b had a notch shape between these two extremes.

These effects of D could be well-explained by the redistribution of the reactant. For clarity, panels d–f of Figure 2 show the distribution of reactants only at the same plane as the twin plane. A large D means that the reactant is quickly replenished at the etched sites, so that the newly exposed atoms would be more susceptible toward further etching, leading to positive feedback. In this case, the relative stability of the facets is the critical factor of the etching selectivity (Figure 2d). In contrast, with the smallest D , meaning that the reactant could not be replenished fast enough, the distribution of the reactant becomes the critical factor, as manifested by the arc-shaped or near-radial distribution of reactants (Figure 2f), eventually leading to the arc-shaped notches.

To further explore the competition among active sites, we selected three sites at each edge to be the preferential etched sites (Figure 2g and Figure S4). The overall trends were the same, in terms of the evolution of the notch shapes and the largest D -focused etching at a few sites (Figure S4a), whereas the smallest D led to roughly equally etched notches (Figure 2g and Movies S1 and S2). With an increased number of active sites, the competition among them became more evident and so was the randomness among the etched and barely etched sites and the varying degrees of etching. In short, the competition among the active sites critically depends on the diffusion of reactants, and a large D tends to focus the etching at a few active sites. Notably, a serrated edge shape was formed under conditions similar to Figure 2g, where six preferential etching sites were present along each edge, closely aligning with the experimental observation (Figure 2h).²⁴

Recently, we also achieve facet-selective etching in triangular Au nanoplates to make holes,²⁵ and the main difference from the edge-selective etching is charge repulsion among the ligand. The repulsion is expected to be the strongest at the lowest curvature sites, and thus, the flat $\{111\}$ facets would have the lowest ligand density. This predisposes the flat regions to preferential etching, particularly the few initial sites after random ligand loss. In comparison, the ligands at the higher curvature sites (edges and corners) are expected to be more stable with less repulsion.

To simulate facet-selective etching, other than assigning ligand effects to each surface atom according to the above-mentioned rule, we selected three areas to be the preferential etching sites, as shown in Figure 3a (pink triangles). With suitable diffusion factor D set to avoid focused etching, simultaneous etching was achieved at the three assigned areas (panels b and c of Figure 3). When l_i assigned to the atoms of the $\{111\}$ facet was 1.20, triangular pits with the same direction of the triangular nanoplate (upright position) appeared at the early stage of etching. With further etching, their size increased and perforated the nanoplate, obtaining holes in the upright position. Specially, with gradually decreased l_i , holes with different shapes were obtained. When $l_i = 1.10$, pits/holes of the inverted triangle were obtained. For the intermediate ligand strength ($l_i = 1.15$), hexagonal holes were obtained. The formation of these differently shaped holes was consistent with previous experimental observations (Figure 3c),²⁵ and the current results provided useful clues for the underlying mechanism.

After extensive studies (Figure S5; see the Supporting Information for more details), we realized that the critical point lies in the choice between etching the atoms with nine

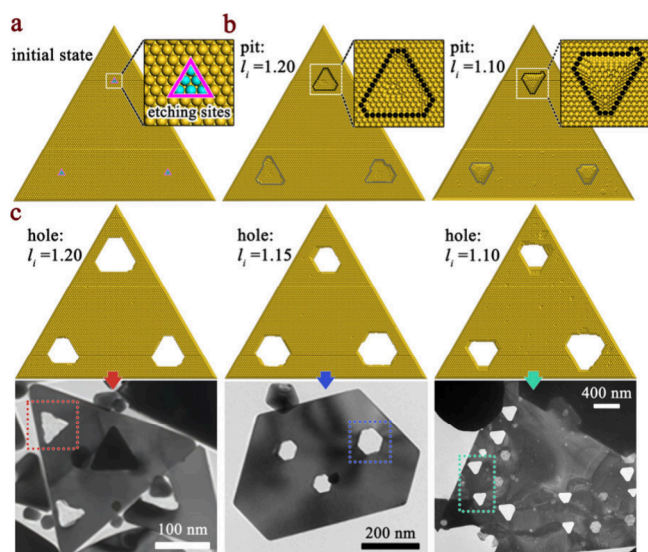


Figure 3. Selective etching at the facet sites of the triangular Au nanoplate under the ARDA condition. In each case, a different ligand effect l_i is assigned to the atoms of the $\{111\}$ facet. The diffusion factor D is properly set as 0.150, so that all the preferential sites would be uniformly etched. (a) Initial configuration of the triangular Au nanoplate, where all surface sites have been assigned ligands and three preferential etch sites are assigned to have weak ligands (six atoms in the pink triangle). (b) Pits at the early stage of etching with $l_i = 1.20$ and 1.10. (c) Holes have different shapes with different l_i , and transmission electron microscopy images are provided for comparison.

bonds without a ligand or the ligand-passivated atoms with six bonds. When an upright triangular pit is initially generated, selecting the former option preserves the pit's shape, allowing it to develop into a hole with upright triangles. In contrast, the latter option causes the shape to first transform into inverted triangles before becoming a hole. When the two types of atoms have similar etching priorities, a hexagonal shape is obtained. **Figure 3** essentially demonstrates that, when all other factors remain constant, variations in l_i modulate the etching sequence, giving holes of a different shape.

In addition to the ARDA condition, we also studied the etching when all of the environmental points had the same and constant amount of reactant (the SCAR condition). Basically, it depicted a scenario with infinite diffusion rates, so that all used reactants were instantaneously replenished. In fact, this was the typical situation adopted in the previous literature. In the absence of ligand under SCAR conditions, atoms with fewer bonding numbers were more easily etched, and the newly exposed atoms after etching always had a bonding number greater than or equal to the etched ones. Hence, the three corners of the Au nanoplate were etched simultaneously, giving rounded structures (**Figure S6a**) similar to that in **Figure 1**. These results were consistent with experimental observations in the literature.

However, in the presence of ligands, the SCAR condition would greatly intensify the competition among the active sites, more so than the cases described above with large D (**Figure 2**). More specifically, the etching was mainly focused on one site among the marked preferential ones, regardless if it was for one site per each edge (**Figure S6b**), many sites per each edge (**Figure S6b**), or many sites on the top facet (**Figure S6c**). For these cases, as soon as the edge or facet site was etched, the

bonding numbers of nearby surface atoms decrease and the newly exposed atoms were not protected by ligands. As a result, the etched sites were more susceptible to further etching, leading to a progressively increasing tendency that focused the etching on one specific site. Obviously, this condition is not conducive to the formation of notches at the edges or holes on the faces. In other words, the SCAR condition is incompatible with the ligand effects, and that is why we use the ARDA condition for the above discussions.

In this work, we successfully simulate the inequivalent etching of initially equivalent sites on triangular Au nanoplates, and the product morphologies are well-aligned with the experimental observations, even to the extent of the detailed shapes of the notches and holes. Most importantly, our results have shown that conventional simulation methods have missed a great deal: The default conditions are valid only when ligands quickly reach adsorption/desorption equilibrium, and reactant diffusion is rapid. This is often not the case for strong ligands, and it would not be right to oversimplify the ligand effects then. Although the detailed effects of ligands are complex, our simulations have shown that treating ligands numerically is an effective approach, yielding results that are well-aligned with experimental observations.

Looking forward, this approach could be easily adapted to study inequivalent growth of crystals, explaining abnormal nanostructures, chiral nanostructures, and even dendritic growth in batteries.

■ ASSOCIATED CONTENT

Supporting Information

The Supporting Information is available free of charge at <https://pubs.acs.org/doi/10.1021/acs.jpcllett.5c01291>.

Movie S1 showing the progression of selective edge etching (AVI)

Movie S2 showing the progression of selective edge etching (AVI)

Simulation details, edge etching results, mechanism of facet etching with a different hole shape, and etching under the SCAR condition (PDF)

■ AUTHOR INFORMATION

Corresponding Author

Hongyu Chen – Department of Chemistry, School of Science and Key Laboratory for Quantum Materials of Zhejiang Province, Research Center for Industries of the Future, Westlake University, Hangzhou 310030, China; Institute of Natural Sciences, Westlake Institute for Advanced Study, Hangzhou 310024, China; orcid.org/0000-0002-5325-9249; Email: chenhongyu@westlake.edu.cn

Authors

Guangyu He – Department of Chemistry, School of Science and Key Laboratory for Quantum Materials of Zhejiang Province, Research Center for Industries of the Future, Westlake University, Hangzhou 310030, China; Institute of Natural Sciences, Westlake Institute for Advanced Study, Hangzhou 310024, China; orcid.org/0000-0002-9054-2764

An Su – Department of Chemistry, School of Science and Key Laboratory for Quantum Materials of Zhejiang Province, Research Center for Industries of the Future, Westlake University, Hangzhou 310030, China; Institute of Natural

Sciences, Westlake Institute for Advanced Study, Hangzhou 310024, China; orcid.org/0000-0001-5187-8727

Qian Wang – Department of Chemistry, School of Science and Key Laboratory for Quantum Materials of Zhejiang Province, Research Center for Industries of the Future, Westlake University, Hangzhou 310030, China; Institute of Natural Sciences, Westlake Institute for Advanced Study, Hangzhou 310024, China

Shi Liu – Department of Chemistry, School of Science and Key Laboratory for Quantum Materials of Zhejiang Province, Research Center for Industries of the Future, Westlake University, Hangzhou 310030, China; Institute of Natural Sciences, Westlake Institute for Advanced Study, Hangzhou 310024, China; orcid.org/0000-0002-8488-4848

Complete contact information is available at:

<https://pubs.acs.org/10.1021/acs.jpcllett.5c01291>

Notes

The authors declare no competing financial interest.

ACKNOWLEDGMENTS

The authors are thankful for the financial support from the National Natural Science Foundation of China: Major Research Plan (Project 92356310), the Leading Innovative and Entrepreneur Team Introduction Program of Zhejiang (Project TD2022004), and the Foundation of Westlake University. The authors thank Westlake University Super-computer Center for the facility support and technical assistance.

REFERENCES

- (1) Gilmer, G. H.; Bennema, P. Simulation of Crystal Growth with Surface Diffusion. *J. Appl. Phys.* **1972**, *43* (4), 1347–1360.
- (2) Hill, A. R.; Cubillas, P.; Gebbie-Rayet, J. T.; Trueman, M.; de Bruyn, N.; Harthi, Z. a.; Pooley, R. J. S.; Attfield, M. P.; Blatov, V. A.; Proserpio, D. M.; Gale, J. D.; Akporiaye, D.; Arstad, B.; Anderson, M. W. CrystalGrower: a generic computer program for Monte Carlo modelling of crystal growth. *Chemical Science* **2021**, *12* (3), 1126–1146.
- (3) Levi, A. C.; Kotrla, M. Theory and simulation of crystal growth. *J. Phys.: Condens. Matter* **1997**, *9* (2), 299–344.
- (4) Mazal, T.; Doherty, M. F. Modeling Impurity-Mediated Crystal Growth and Morphologies of Centrosymmetric Molecules. *Cryst. Growth Des.* **2023**, *23* (1), 369–379.
- (5) van Enkevort, W. J. P.; Los, J. H. “Tailor-Made” Inhibitors in Crystal Growth: A Monte Carlo Simulation Study. *J. Phys. Chem. C* **2008**, *112* (16), 6380–6389.
- (6) Gandin, C.-A.; Desbiolles, J.-L.; Rappaz, M.; Thevoz, a. P. A three-dimensional cellular automaton-finite element model for the prediction of solidification grain structures. *Metallurgical and Materials Transactions A* **1999**, *30* (12), 3153–3165.
- (7) Boerrigter, S. X. M.; Josten, G. P. H.; van de Streek, J.; Hollander, F. F. A.; Los, J.; Cuppen, H. M.; Bennema, P.; Meekes, H. MONTY: Monte Carlo Crystal Growth on Any Crystal Structure in Any Crystallographic Orientation; Application to Fats. *J. Phys. Chem. A* **2004**, *108* (27), 5894–5902.
- (8) Broad, A.; Darkins, R.; Duffy, D. M.; Ford, I. J. Calcite Kinks Grow via a Multistep Mechanism. *J. Phys. Chem. C* **2022**, *126* (37), 15980–15985.
- (9) Kaushik, A.; Marvaniya, K.; Kulkarni, Y.; Bhatt, D.; Bhatt, J.; Mane, M.; Suresh, E.; Tothadi, S.; Patel, K.; Kushwaha, S. Large-area self-standing thin film of porous hydrogen-bonded organic framework for efficient uranium extraction from seawater. *Chem.* **2022**, *8* (10), 2749–2765.

- (10) Tong, J.; de Bruyn, N.; Alieva, A.; Legge, E. J.; Boyes, M.; Song, X.; Walsinghe, A. J.; Pollard, A. J.; Anderson, M. W.; Vetter, T.; Melle-Franco, M.; Casiraghi, C. Crystallization of molecular layers produced under confinement onto a surface. *Nat. Commun.* **2024**, *15* (1), 2015.

- (11) Ci, P.; Zhao, Y.; Sun, M.; Rho, Y.; Chen, Y.; Grigoropoulos, C. P.; Jin, S.; Li, X.; Wu, J. Breaking Rotational Symmetry in Supertwisted WS₂ Spirals via Moiré Magnification of Intrinsic Heterostrain. *Nano Lett.* **2022**, *22* (22), 9027–9035.

- (12) Zhao, Y. Z.; Zhang, C. Y.; Kohler, D. D.; Scheeler, J. M.; Wright, J. C.; Voyles, P. M.; Jin, S. Supertwisted spirals of layered materials enabled by growth on non-Euclidean surfaces. *Science* **2020**, *370* (6515), 442–445.

- (13) Libbrecht, K. G. Snow Crystals. *arXiv.org, e-Print Arch., Condens. Matter* **2021**, arXiv:1910.06389.

- (14) Libbrecht, K. G. A Dual Diffusion Chamber for Observing Ice Crystal Growth on c-Axis Ice Needles. *arXiv.org, e-Print Arch., Condens. Matter* **2014**, arXiv:1405.1384.

- (15) Libbrecht, K. G. An experimental apparatus for observing deterministic structure formation in plate-on-pedestal ice crystal growth. *arXiv.org, e-Print Arch., Condens. Matter* **2015**, arXiv:1503.01019.

- (16) Ji, J.; Chen, Z.; Jiang, T.; Feng, Y.; Chen, H. Two-dimensional active surface growth of Ag nanoplates. *Inorganic Chemistry Frontiers* **2024**, *11* (14), 4288–4296.

- (17) Su, A.; Wang, Q.; Huang, L.; Zheng, Y.; Wang, Y.; Chen, H. Gold nanohexagrams via active surface growth under sole CTAB control. *Nanoscale* **2023**, *15* (36), 14858–14865.

- (18) Xia, X.; Xie, S.; Liu, M.; Peng, H.-C.; Lu, N.; Wang, J.; Kim, M. J.; Xia, Y. On the role of surface diffusion in determining the shape or morphology of noble-metal nanocrystals. *Proc. Natl. Acad. Sci. U. S. A.* **2013**, *110* (17), 6669–6673.

- (19) Gravner, J.; Griffeath, D. Modeling snow crystal growth II: A mesoscopic lattice map with plausible dynamics. *Physica D: Nonlinear Phenomena* **2008**, *237* (3), 385–404.

- (20) Gravner, J.; Griffeath, D. Modeling snow-crystal growth: A three-dimensional mesoscopic approach. *Phys. Rev. E* **2009**, *79* (1), No. 011601.

- (21) Libbrecht, K. G. A Quantitative Physical Model of the Snow Crystal Morphology Diagram. *arXiv.org, e-Print Arch., Condens. Matter* **2019**, arXiv:1910.09067.

- (22) Feng, Y.; He, J.; Wang, H.; Tay, Y. Y.; Sun, H.; Zhu, L.; Chen, H. An Unconventional Role of Ligand in Continuously Tuning of Metal–Metal Interfacial Strain. *J. Am. Chem. Soc.* **2012**, *134* (4), 2004–2007.

- (23) Feng, Y.; Wang, Y.; He, J.; Song, X.; Tay, Y. Y.; Hng, H. H.; Ling, X. Y.; Chen, H. Achieving Site-Specificity in Multistep Colloidal Synthesis. *J. Am. Chem. Soc.* **2015**, *137* (24), 7624–7627.

- (24) He, B.; Wang, Y.; Zhang, M.; Xu, Y.; Zheng, Y.; Liu, X.; Wang, H.; Chen, H. Serrated Au Nanoplates via the Sharpening Etching Mode. *Chem. Mater.* **2022**, *34* (18), 8213–8218.

- (25) Hu, H.; Wang, Y.; Wang, Q.; Peng, X.; Su, A.; Wang, H.; Chen, H. Boring holes in Au nanoplates by active surface etching. *Nano Research* **2024**, *17* (9), 8610–8617.

- (26) Xiao, R.; Jia, J.; Wang, R.; Feng, Y.; Chen, H. Strong Ligand Control for Noble Metal Nanostructures. *Acc. Chem. Res.* **2023**, *56* (12), 1539–1552.

- (27) Forty, A. J. The growth of cadmium iodide crystals. 1. Dislocations and spiral growth. *Philos. Mag.* **1952**, *43* (336), 72.

- (28) Forty, A. J. The growth of cadmium iodide crystals. 2. A study of the heights of growth steps on cadmium iodide. *Philos. Mag.* **1952**, *43* (339), 377.

- (29) Combe, N.; Jensen, P.; Pimpinelli, a. A. Changing Shapes in the Nanoworld. *Phys. Rev. Lett.* **2000**, *85* (1), 110–113.

- (30) Behler, J.; Parrinello, M. Generalized Neural-Network Representation of High-Dimensional Potential-Energy Surfaces. *Phys. Rev. Lett.* **2007**, *98* (14), No. 146401.

- (31) He, G.; Wang, R.; Fan, J.; Liu, S.; Chen, H. In silico investigation on the twisting of gold nanowires. *Materials Today Communications* **2022**, *33*, No. 104319.
- (32) Huang, S.-D.; Shang, C.; Kang, P.-L.; Zhang, X.-J.; Liu, Z.-P. LASP: Fast global potential energy surface exploration. *WIREs Computational Molecular Science* **2019**, *9* (6), No. e1415.
- (33) Dahl, S.; Logadottir, A.; Jacobsen, C. J. H.; Nørskov, J. K. Electronic factors in catalysis: the volcano curve and the effect of promotion in catalytic ammonia synthesis. *Applied Catalysis A: General* **2001**, *222*, 19–29.
- (34) Logadottir, A.; Rod, T. H.; Nørskov, J. K.; Hammer, B.; Dahl, S.; Jacobsen, C. J. H. The Brønsted–Evans–Polanyi Relation and the Volcano Plot for Ammonia Synthesis over Transition Metal Catalysts. *J. Catal.* **2001**, *197* (2), 229–231.
- (35) Medford, A. J.; Vojvodic, A.; Hummelshøj, J. S.; Voss, J.; Abild-Pedersen, F.; Studt, F.; Bligaard, T.; Nilsson, A.; Nørskov, J. K. From the Sabatier principle to a predictive theory of transition-metal heterogeneous catalysis. *J. Catal.* **2015**, *328*, 36–42.
- (36) Sekerka, R. F. Role of instabilities in determination of the shapes of growing crystals. *J. Cryst. Growth* **1993**, *128* (1–4), 1–12.
- (37) Gladstein, A.; Aramanda, S. K.; Shi, L.; Landini, J.; Goettsch, J.; Reese, C.; Sahu, B.; Xiao, X.; Hunter, A.; Thornton, K.; Shahani, A. J.; Taub, A. I. Direct evidence of the formation mechanisms of TiC nanoparticles and Al₃Ti intermetallics during synthesis of an Al/TiC metal matrix nanocomposite. *Acta Mater.* **2024**, *277*, No. 120189.
- (38) Yang, Z.; Zhang, J.; Zhang, L.; Fu, B.; Tao, P.; Song, C.; Shang, W.; Deng, T. Self-Assembly in Hopper-Shaped Crystals. *Adv. Funct. Mater.* **2020**, *30* (26), No. 1908108.
- (39) Li, Y. W.; Lin, H. X.; Zhou, W. J.; Sun, L.; Samanta, D.; Mirkin, C. A. Corner-, edge-, and facet-controlled growth of nanocrystals. *Science Advances* **2021**, *7* (3), No. eabf1410.
- (40) Maksym, P. A. Fast Monte Carlo simulation of MBE growth. *Semicond. Sci. Technol.* **1988**, *3* (6), 594–596.
- (41) Bortz, A. B.; Kalos, M. H.; Lebowitz, J. L. A new algorithm for Monte Carlo simulation of Ising spin systems. *J. Comput. Phys.* **1975**, *17* (1), 10–18.
- (42) Scarabelli, L.; Sun, M.; Zhuo, X.; Yoo, S.; Millstone, J. E.; Jones, M. R.; Liz-Marzán, L. M. Plate-Like Colloidal Metal Nanoparticles. *Chem. Rev.* **2023**, *123* (7), 3493–3542.
- (43) Tian, J.; Lin, D.; Li, X.; Wang, K.; Yu, B.; Li, M.; Hou, S.; Li, Z.; Chen, Q. The Growth and Shape Evolution of Indium Nanoplates Studied by In Situ Liquid Cell TEM. *Small* **2024**, *20* (46), No. 2400680.
- (44) Lofton, C.; Sigmund, W. Mechanisms Controlling Crystal Habits of Gold and Silver Colloids. *Adv. Funct. Mater.* **2005**, *15* (7), 1197–1208.
- (45) Aherne, D.; Ledwith, D. M.; Gara, M.; Kelly, J. M. Optical Properties and Growth Aspects of Silver Nanoprisms Produced by a Highly Reproducible and Rapid Synthesis at Room Temperature. *Adv. Funct. Mater.* **2008**, *18* (14), 2005–2016.
- (46) Wang, Y.; He, J.; Liu, C.; Chong, W. H.; Chen, H. Thermodynamics versus Kinetics in Nanosynthesis. *Angew. Chem., Int. Ed.* **2015**, *54* (7), 2022–2051.